Reconstruction of DEMs From ERS-1/2 Tandem Data in Mountainous Area Facilitated by SRTM Data

Mingsheng Liao, Teng Wang, Lijun Lu, Wenjun Zhou, and Deren Li

Abstract—A new approach is presented in this paper to produce Digital Elevation Model (DEM) in mountainous areas with steep slope using ERS-1/2 tandem data. In order to reduce the impact of phase errors on the Interferometric Synthetic Aperture Radar (InSAR)-generated DEM, an external DEM such as that from Shuttle Radar Topography Mission (SRTM) is utilized in this approach. The proposed algorithm includes two steps: The first step is to model and remove phase trends with a linear regression analysis before converting phase to height; the second step is to filter unreliable height points before interpolating the DEM from the InSAR height map. The critical points are the following: 1) determining the one-to-one correspondence between the interferogram and the SRTM DEM before knowing the InSAR-derived elevation values and 2) estimating the elevation range of every pixel from SRTM DEM. To solve the first problem, an iteratively geocoding algorithm is performed. A DEM interpolation error model solves the second one. For InSAR data processing, the SRTM DEM is not only usable for modeling systematic phase errors but also for filtering gross height errors. The experiments in Zhangbei and the Three Gorges areas in China show that our approach has improved the accuracy of the resulting DEMs significantly without any ground control points.

Index Terms—Digital elevation model, geocoding, linear regression analysis, Shuttle Radar Topography Mission (SRTM), Synthetic Aperture Radar (SAR) interferometry.

I. INTRODUCTION

ONE OF THE most important applications of Interferometric Synthetic Aperture Radar (InSAR) technology is the generation of Digital Elevation Models (DEMs). The DEM generation is based on the measurement of phase difference between two complex radar signals, i.e., the range difference between the sensor and the targets. Using the range difference and sensor orbital parameters, one can derive the elevation of the illuminated surface [1].

It is well considered that phase error is one of the main error sources of InSAR-generated DEM with repeat-pass satellite mode [2]. The phase error consists of three parts: 1) phase trends caused by orbital errors in the flattened interferogram; 2) errors caused by decorrelation and thermal noise; and 3) atmospheric phase screen (APS) difference between master and slave images.

When a DEM is constructed from interferogram, the phase trends will convert to systematic elevation error, which can be reduced or removed using ground control points (GCPs) in data processing [3]. However, it is not always easy to identify GCPs in some wild areas from SAR images.

For the phase errors caused by geometrical and temporal decorrelation, the accuracy of the elevation is affected by these accidental and/or gross errors, particularly for the repeat-pass satellite mode [4]. Although the accidental phase errors can be reduced by filtering or averaging the interferogram, the gross errors are difficult to remove.

The model of atmospheric effect errors in interferogram is very complex. It can be divided into topographic dependent and independent parts [5], [6]. Without knowledge of terrain information before DEM generation, the topographic dependent atmospheric errors are very difficult to remove. Ferretti *et al.* averaged multibaseline InSAR DEMs using wavelet approach for weighting to remove atmospheric effect in DEMs [7]. Although the accuracy of the resulted DEM can be very good, the requirement of multiple data sets is hard to meet in most cases of topographic mapping.

From geometry formulation of InSAR, the impact of all these phase errors is in inverse proportion to the length of normal baseline. The height errors from interferometric phase errors are reduced when the normal baseline is long, but the signal-to-noise ratio of interferogram decreases with the baseline increasing [8]. Moreover, the height change that leads to a 2π change in interferometric phase (height ambiguity) is also inversely proportional to the length of normal baseline. Therefore, in mountainous areas, steep terrain often causes phase aliasing in interferogram with long baselines, which make it difficult to unwrap the phase.

On the other hand, in the case of short normal baseline, although the interferogram may be unwrapped easily with high coherence and low local phase frequency, the errors mentioned above will make the resulted DEM far from application. Additional, errors from decorrelation and thermal noise may convert to gross height errors which destroy the interpolated DEM. Therefore, to get a good result from short baseline data set, the restraint of phase error is strongly required.

As a consequence of the analysis above, the selection between long and short baseline data sets for mountainous area DEM generation is in a dilemma. However, when certain prior knowledge about terrain of the interested area is obtained, most of the difficulties could be overcome.

Seymour and Cumming presented an approach to use coarse low-quality DEMs reducing local phase bandwidth of interferograms. Lower local fringe frequency makes the probability of

residues lower and the procedure of phase unwrapping easier [9]. Eineder and Adam used external DEMs to reduce the search range of elevation when using a maximum likelihood estimator to simultaneously unwrap, geocode, and fuse SAR interferograms from different viewing geometries into one DEM [10]. Sang-Ho *et al.* presented an approach to merge the high- and low-resolution InSAR-derived DEMs in the frame of a prediction-error filter [11]. All the works above offered clues of making use of existed low-resolution DEMs in procedures of InSAR DEM generation.

In this paper, the usage of external low-resolution DEMs, such as Shuttle Radar Topography Mission (SRTM) DEM data, is concerned from a novel aspect. As an external DEM data set here, the SRTM DEM is used with the following two purposes: One is to model the linear part of phase errors (trends) that are relative to azimuth, range, and height in radar's slant range space by linear regression analysis; the other is to remove the unreliable height points before DEM reconstruction.

Facilitated by SRTM DEM, the systematic errors in interferogram can be removed. Although the accuracy of SRTM DEM is not as high as GCPs, depending on the amount and distribution of the elevation grids, our work shows that the estimation of phase trends coefficients is reliable from statistic perspective. Besides the systematic error, the pixels with gross errors can be filtered as well, depending on the estimated elevation range.

This paper is organized as follows. Section II reviews the error model in interferogram from the view of a linear model, which depends on azimuth, range coordinates, and height. Section III describes the novel procedures of our approach, including correspondence determination between interferogram and SRTM DEM, linear regression analysis and unreliable height point removal. Section IV shows the experiment results in Zhangbei and the Three Gorges areas with steep terrain and the assessment of resulted DEMs. Finally, Section V gives the conclusions and comments for future work.

II. LINEAR MODEL OF PHASE ERRORS IN INTERFEROGRAM

InSAR geometry and error model of DEM generation have been discussed in many publications [1]–[5]. In this section, we review the interferometric phase errors from the view of a linear model. The variable in this model is coordinates in azimuth, range directions, and phase calculated from SRTM DEM.

The interferometric phase of a pixel is caused by the following:
1) sensor-target range difference between sensors;
2) possible physical and geometric character changes of ground scatters;
3) changes of atmosphere between two data acquire times;
4) thermal noise, etc.

As shown in the following equation, the interferometric phase consists of the above four terms, which are written as ϕ_r, ϕ_t, ϕ_a, and ϕ_n, respectively.

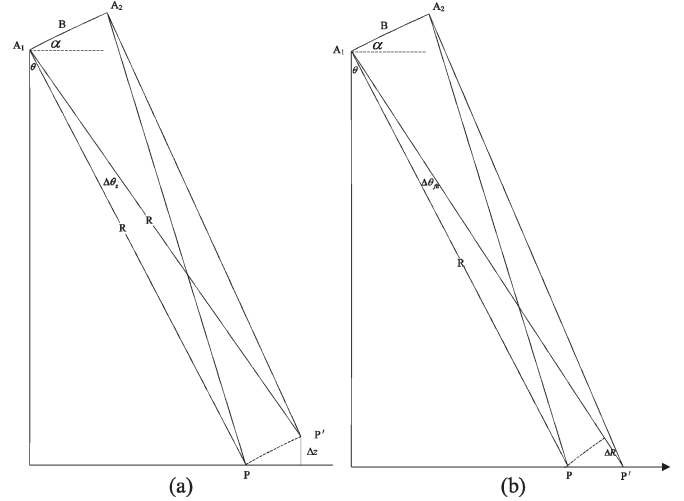$$\phi = \phi_r + \phi_t + \phi_a + \phi_n. \tag{1}$$

Fig. 1. Phase difference geometry. (a) Geometry of phase difference from the height difference with an identical slant range. (b) Geometry of phase difference from the slant range difference with an identical height.

Because we focus on InSAR DEM generation in this paper, ϕ_t is neglected by using ERS-1/2 tandem data sets due to their one-day interval.

ϕ_r can be divided into two parts. Fig. 1(a) shows the phase difference resulting from the height difference with an identical slant range, and Fig. 1(b) shows that resulting from the slant range difference with an identical height. In Fig. 1(a) and (b), A1 and A2 represent two SAR sensors, B is the baseline, R is the range in the line of sight from ground target to the SAR sensor, θ is the incidence angle, and a is the angle of baseline with respect to the horizontal plane.

As shown in Fig. 1(a) and (b), the phase difference, i.e., $\Delta\phi_z$ and $\Delta\phi_{\text{flt}}$, can be written in the following equations, respectively:

$$\phi_z = -\frac{4\pi}{\lambda}\frac{B\cos(\theta - \alpha)\Delta z}{R\sin\theta} \tag{2}$$

$$\phi_{\text{flt}} = -\frac{4\pi}{\lambda}\frac{B\cos(\theta - \alpha)\Delta R}{R\tan\theta}. \tag{3}$$

Here, Δz is the height difference of target on ground with an identical slant range and ΔR is the slant range difference of target on ground with an identical height. Equation (3) means that flatten earth can also cause phase changes. In InSAR processing, this part of phase differences can be modeled and removed as reference phase in the "flatten earth" step using orbital information.

However, errors in orbital parameters may cause additive phase trends in the flattened interferogram. Because most of orbital errors are systematic and relative to SAR coordinates in azimuth and range directions, we can model the phase trends as

$$\phi_{\text{trd}} = c + l_1 i + l_2 j. \tag{4}$$

In (4), c is a constant, i and j mean the SAR image coordinates in azimuth and range directions, respectively, and l_1 and l_2 are linear coefficients of phase trends.

Using the model shown as (4), the mean value of atmospheric effect can be estimated as well. However, as mentioned in Section I, in mountainous areas, except from azimuth and range directions, the APS difference between master and slave images is also partly relative to terrain. Therefore, we modify the model described in (4) as

$$\phi_{\text{trd}} = c + l_1 i + l_2 j + l_3 \phi_z. \tag{5}$$

Now, we can rewrite (1) as

$$\phi = \phi_z + \phi_{\text{flt}} + \phi_{\text{trd}} + \phi_n + \phi_{\text{rsd}}. \tag{6}$$

In this phase model, ϕ_{flt} was removed in the generation of interferogram and ϕ_z can be obtained from SRTM DEM. In addition, ϕ_n is the phase noise and ϕ_{rsd} is the APS difference residue phase.

After ϕ_{flt} and ϕ_z are subtracted from the interferogram, the phase difference can be written as

$$\Delta\phi = \phi_{\text{trd}} + \phi_{\text{err}} + \phi_n + \phi_{\text{rsd}}. \tag{7}$$

Here, ϕ_{err} is the SRTM DEM elevation error in phase. Because SRTM was a single-pass mission, the influence of uncertainty of baseline and APS difference has been highly reduced [12]. The assumption that the errors of SRTM DEM fit a normal distribution of zero mean and constant standard deviation in the range of test area is performed. Also, the impact of ϕ_n and ϕ_{rsd} is neglected in the linear regression analysis due to the large number of regression samples and selective strategy described in the next section.

Except the modeled phase trends errors, the gross errors in some pixels due to phase noise, phase unwrapping, and/or radar shadow in InSAR-derived height map may exist, which will reduce the accuracy of DEM product. This part of errors can be handled by estimating a reasonable elevation range from SRTM DEM.

From the above analysis, the motive of our algorithm is obvious. First, the coefficients $c, l_n (n = 1, 2, 3)$ are regressed, and then, the threshold to filter gross errors from unwrapped interferogram and SRTM DEM is estimated. These estimations are performed on radar's slant range space and object space, i.e., map geometry space, respectively.

III. METHODOLOGY

As described in the previous sections, the working flow of our approach is shown in Fig. 2. Phase difference between the interferogram and the SRTM DEM is calculated. Then, the linear regression analysis is performed to model the systematic errors before the phase-to-height conversion. Finally, on the height map, a certain threshold is estimated from the SRTM DEM to remove pixels with gross errors.

Although the data processing looks straightforward, still some technical details need to be well considered. The most important two problems are how to get the one-to-one correspondence between interferogram and the SRTM DEM before knowing the elevation values derived from InSAR and how to
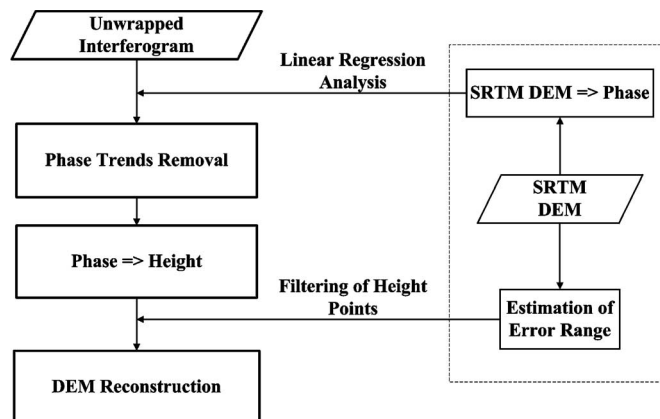

Fig. 2.   Flow of our approach.

estimate the elevation range of every pixel from the SRTM DEM. The solutions are shown as follows.

A. Correspondence Determination Between Interferogram and SRTM DEM

In order to model the systematic errors of the InSAR DEM, the difference between the InSAR and SRTM data should be calculated. This difference can be described in two spaces: the object space showing the height difference and the radar's slant range space representing the phase difference.

If the height difference is measured, the unwrapped interferogram should be converted to a height map and georeferenced into the object space. However, precise geocoding requires every pixel's elevation [13]. The height calculated from the interferogram is far off from true value before removing the phase trends and obtaining the absolute phase. Thus, the horizontal errors caused by geocoding make the measurement of the height difference very inaccurate.

Although from the SRTM DEM, we can obtain every grid point's coordinates in the SAR image, the phase still needs to be resampled from the interferogram. Therefore, the problem is that we cannot directly get a one-to-one correspondence between the interferogram and the SRTM DEM in a forward way, that is, from the azimuth and range direction to geographic coordinates or the backward way either.

In our algorithm, the solution is using the SRTM DEM elevation to modify the ellipsoid parameters, i.e., the semimajor and semiminor axes, and iteratively approach each pixel's SRTM DEM elevation. After the procedure converging, the SRTM elevation can be converted to the interferometric phase.

Delft Object-oriented Radar Interferometric Software (Doris)'s phase-to-height ambiguity algorithm [14] is adopted to compute the corresponding SRTM DEM elevation of every image pixel and other parameters. This procedure is iteratively performed for each pixel as the following steps.

1) Use the azimuth coordinates and orbital parameters to locate the SAR positions of the master and slave images.
2) Set current height to be zero as an initialized value.
3) Modify ellipse parameters using the current height.

4) Compute the latitude and longitude for each pixel using Doppler equation, slant range equation, and earth ellipse equation.

5) Calculate the parameters in (2) such as the incidence angle, the sensor-to-target range, and the normal baseline corresponding to the current height.

6) Interpolate bilinearly the current height from SRTM DEM grid. If the elevation value is void, neglect this pixel and go to the next pixel of the interferogram.

7) If the difference between current and previous heights is less than a threshold initially set, the procedure halts. Otherwise, go back to steps 3) to 6).

Since the SRTM DEMs are generated with radar interferometric technique, missing elevation values, i.e., voids, exist in the data sets. In this algorithm, the voids were discarded due to the large number of regression samples.

Because some targets on ground have the same ranges to the sensor, mapping from radar coordinate system to earth is not a unique transformation, particularly in mountainous areas. If the number of the iterations reaches a presetting value and the height has not converged yet, this pixel will be discarded as the relationship between its SAR coordinate and the SRTM elevation cannot be reconstructed in the object space. Thus, only the pixels with stable and valid SRTM elevation values are selected for linear regression analysis.

B. Linear Regression Analysis

Considering that the phase difference for pixels with low coherence may be far off from our model, a certain coherence threshold should be set to discard these pixels. A trial-and-error method is used in this paper.

Excluding the residue of atmospheric effects, the power of phase noise ϕ_n can be estimated from the absolute value of the coherence $|\hat{\gamma}|$ [15]:

$$E\left[(\phi - \phi_0)^2\right] = \frac{1 - |\hat{\gamma}|^2}{2n_l|\hat{\gamma}|^2}. \tag{8}$$

Here, n_l is the multilook number, ϕ_0 is the noise-free phase value, and $E[(\phi - \phi_0)^2]$ is a kind of absolute coherence estimation value. In order to reduce the phase noise by averaging the interferogram, n_l is set to 20 (10 in azimuth and 2 in range) in this paper. The coherence threshold was set as 0.2 experientially in this paper to discard low coherence pixels and offer enough regression samples.

Once the pixels of the multilooked interferogram as well as their phase difference $\Delta\phi$ are determined, the linear regression equations can be written as

$$\begin{bmatrix} i_1 & j_1 & \phi_{z1} & 1 \\ \cdots & \cdots & \cdots & \cdots \\ i_n & j_n & \phi_{zn} & 1 \end{bmatrix} \begin{bmatrix} l_1 \\ l_2 \\ l_3 \\ c \end{bmatrix} = \begin{bmatrix} \Delta\phi_1 \\ \Delta\phi_2 \\ \cdots \\ \Delta\phi_n \end{bmatrix} \tag{9}$$

where n means the number of phase difference samples. Then, the coefficients c, l_1, l_2, l_3 are derived by a least-square estimation, as shown in (9).
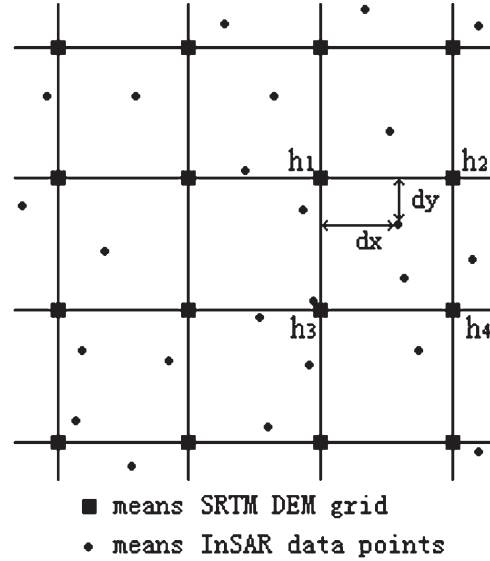

Fig. 3.   Sketch of SRTM elevation interpolation.

TABLE I
BASIC INFORMATION OF DATA SETS

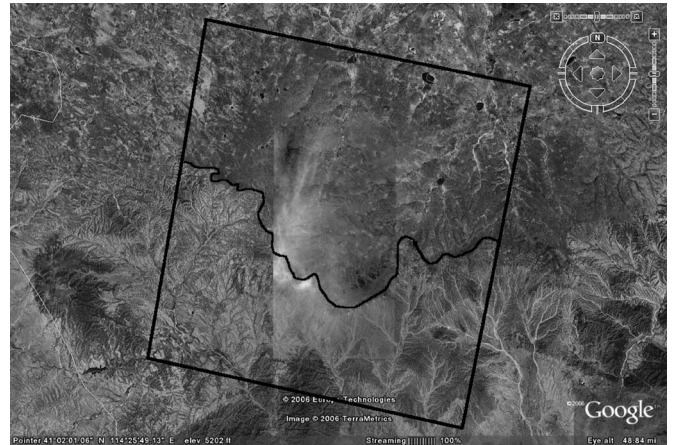| Zhangbei Data Set. TRACK: 32 FRAME: 2781			
ERS1 Orbit	**ERS2 Orbit**	**ERS1-2 Date**	**$|B_n|$**
32585	12912	08-09/10/97	287
Three Gorges Data Set. TRACK: 32 FRAME:2979			
ERS1 Orbit	**ERS2 Orbit**	**ERS1-2 Date**	**$|B_n|$**
23610	03937	20-21/01/96	16

Fig. 4.   Sketch of our test site from Google Earth.

In avoiding the effect of phase unwrapping errors, the regression procedure is also performed iteratively. When the phase trends are estimated, the statistics of residue phase are considered. The pixels with residue phase values larger than two times of standard deviation are removed, and the phase trends are estimated again until the number of the pixels with larger phase residue is less than a certain value, for example, 1% of the total interferogram pixels. Then, the phase trends can be modeled as described in (5). Using this model, the phase trends are removed pixel by pixel across the whole interferogram before the phase-to-height conversion.
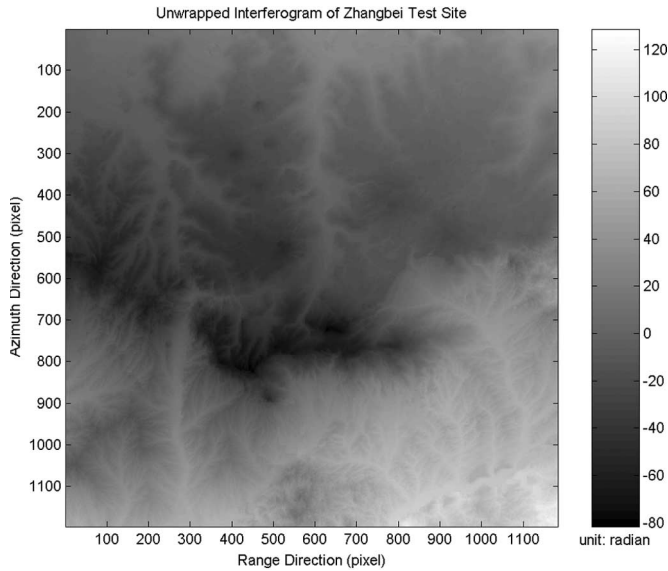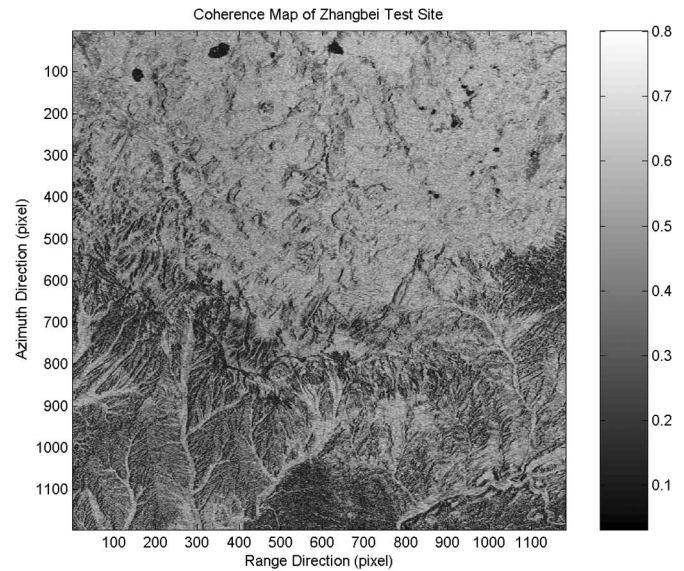
Fig. 5. Unwrapped interferogram of Zhangbei data set.

Fig. 6. Coherence map of Zhangbei data set.

C. Filtering of Unreliable Height Points

After removing the phase trends, the unwrapped interferogram can be converted to a height map by using the iterative procedure described above, except for step 6). Here, the height should be calculated from the following equation, which can be inferred from (2):

$$z = -\frac{\phi_z \lambda R \sin \theta}{4\pi B \cos(\theta - \alpha)}. \tag{10}$$

Since geocoding can be done in this procedure, the longitude, latitude, and height referenced to WGS84 are obtained for each pixel. Then, the threshold to remove pixels with gross height errors is determined depending on the location in the SRTM DEM elevation grid.

Based on Chebyshev theorem, no matter what distribution of the errors fits, the probability that any error is within the interval of $\mu \pm 4\delta$ is at least 94%. μ and δ are the mean and standard deviation here [16]. Therefore, we set four times of the SRTM elevation error as the criteria to remove unreliable pixels. The absolute height difference between InSAR-resulted height points and corresponding SRTM elevation is considered. Only the points with smaller height difference than the threshold are used to reconstruct DEM. The difficulty here is how to estimate error standard deviation of the SRTM DEM in the location of each interferogram pixel.

The SRTM height values are interpolated using a bilinear interpolation, as shown in the following equation, which is based on the location of pixels in interferogram, as shown in Fig. 3:

$$h_i = (1 - dx) \cdot (1 - dy) \cdot h_1 + dx \cdot (1 - dy) \cdot h_2$$
$$+ (1 - dx) \cdot dy \cdot h_3 + dx \cdot dy \cdot h_4. \tag{11}$$

Here, h_1 to h_4 are height values of grid nodes 1 to 4. h_i is the interpolated height value. dx and dy are the distances
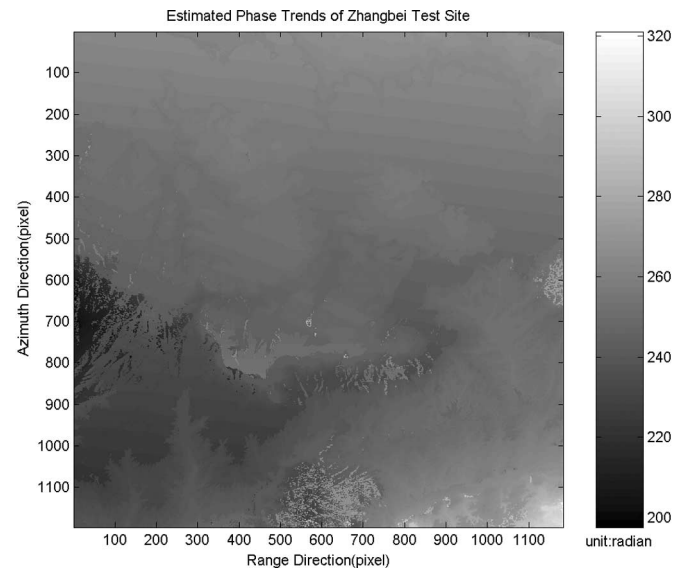

Fig. 7. Estimated phase trends of Zhangbei data set.

from the interpolated height point to the upper left grid node in x- and y-axes which are normalized to 1. The error deviation of the interpolated height can be expressed from the deviation of the grid node and dx, dy as

$$\delta_i^2 = [(1 - dx) \cdot (1 - dy)]^2 \cdot \delta_{\text{nod}}^2 + [dx \cdot (1 - dy)]^2 \cdot \delta_{\text{nod}}^2$$
$$+ [(1 - dx) \cdot dy]^2 \cdot \delta_{\text{nod}}^2 + [dx \cdot dy]^2 \cdot \delta_{\text{nod}}^2 \tag{12}$$

where δ_i^2 is the deviation of interpolated height and δ_{nod}^2 is the deviation of grid nodes of the SRTM DEM. To estimate δ_i^2, δ_{nod}^2 should first obtained. The experiential model (13) from [16] is adapted to get δ_{nod}^2 in (12):

$$\delta_{\text{Surf}}^2 = \frac{4}{9}\delta_{\text{nod}}^2 + \frac{5}{3}\delta_T^2 \tag{13}$$
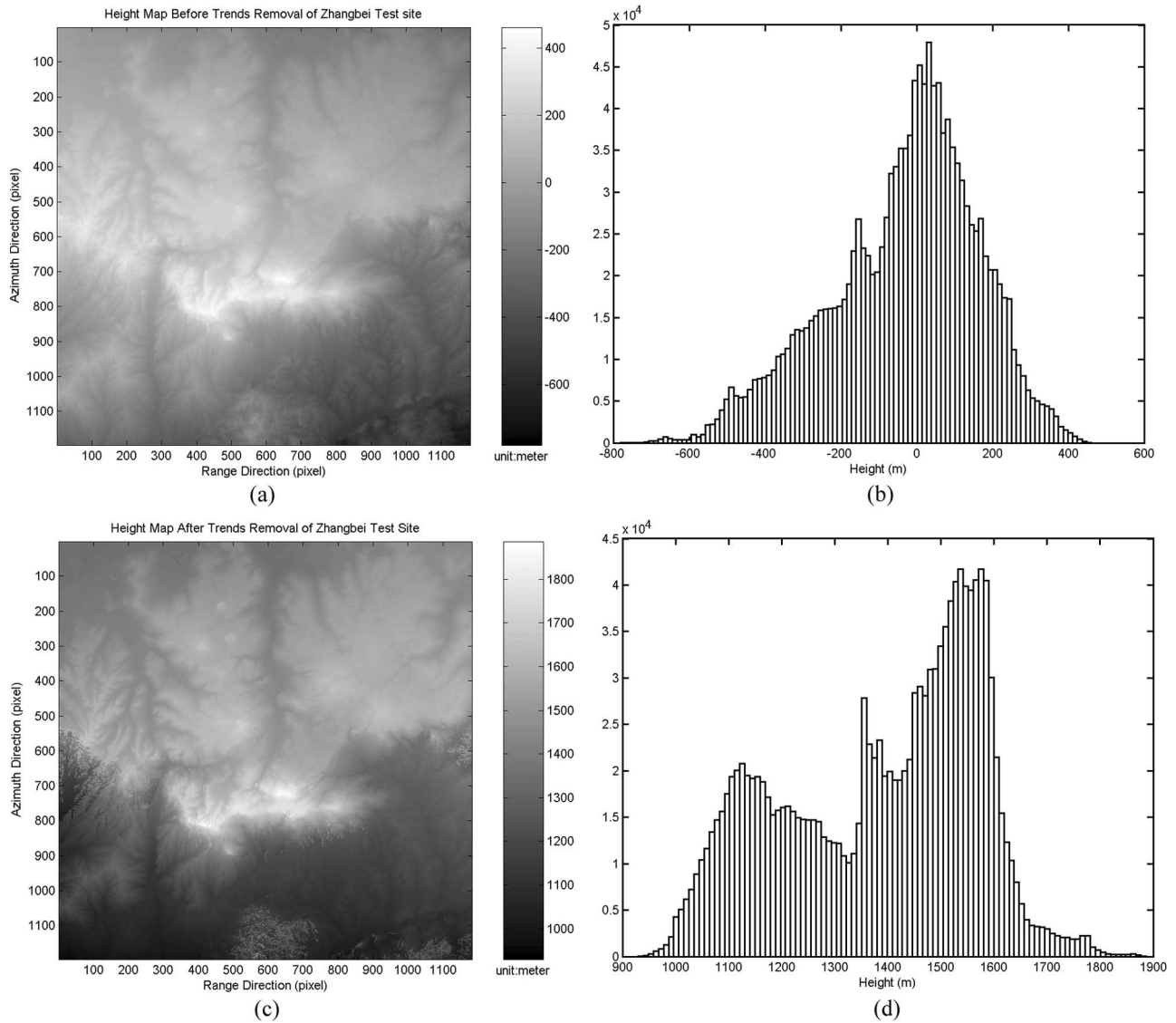
Fig. 8.   Height maps and their histograms before and after removing phase trends of Zhangbei data set. (a) Height map before phase trends removal. (b) Histogram of (a). (c) Height map after phase trends removal. (d) Histogram of (c).

where δ_{Surf}^2 is the mean value of elevation deviation on the bilinear surface and δ_T^2 is the reduced accuracy due to the linear model to express the real surface. The estimation of δ_T^2 is very complicated, which depends on the mean slope of terrain. If the values of δ_{Surf}^2 and δ_T^2 are obtained, the interpolated SRTM elevation error δ_i can be estimated from (12) and (13). The detail of getting δ_{Surf}^2 and δ_T^2, which depend on the test sites, will be presented in the next section

Because the height threshold for each pixel of interferogram needs to be estimated from the SRTM DEM grid, the voids of SRTM DEM should be removed before this procedure by a 3×3 moving window using the following equation, which was applied to the entire study area:

$$\frac{1}{n} \sum h_i (i = 1, 2, \ldots n) \qquad (14)$$

where n means number of valid height points in the window.

Then, the elevation difference between the interferogram and the SRTM DEM is obtained, and the pixel with this difference over the estimated threshold is removed.

Finally, the resulted DEM is interpolated from the filtered height map.

IV. EXPERIMENTAL RESULTS

Two pairs of ERS-1/2 tandem images in different areas are chosen as our test data sets. The basic information of these data sets is summarized in Table I.

The interferograms are averaged with the factor of ten in azimuth and two in range. Flynn's minimum discontinuity method was used for phase unwrapping because of its global minimum L-1 normal solution [17], [18].

The threshold to filter unreliable height points was estimated depending on the accuracy assessment of SRTM DEM and terrain undulation of the test sites.
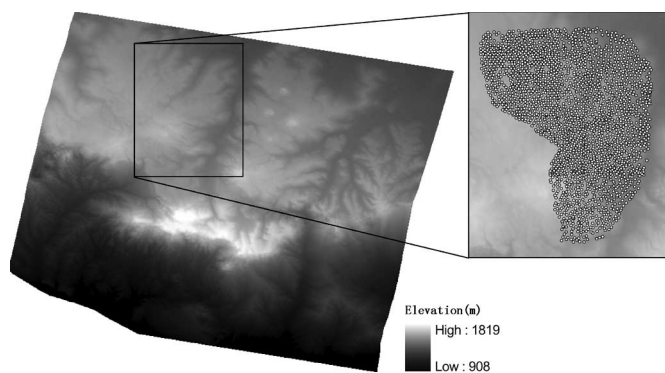
Fig. 9. Resulted DEM of Zhangbei data set with 2692 vector check points from aerial photogrammetry.

Fig. 10. Comparison of errors on check points between traditional InSAR technology, SRTM DEM, and our approach.

The expected vertical accuracy is about 16 m (at 90% confidence) for the 1 arc-second SRTM DEM released for the U.S. territories [19]. For the areas out of the U.S., the resolution of the SRTM DEM is reduced to 3 arc-seconds and the accuracy should be lower than 16 m. By considering the steep slopes in our test sites, we assume the standard deviation of SRTM DEM error δ^2_{Surf} as 50 m and δ^2_T as 10 m. δ^2_{nod} was obtained from (13). Then, the threshold of every InSAR height points was determined by four times of the standard deviation. The results in these two test sites are shown as follows.

A. Zhangbei Test Site

Zhangbei area locates in north–west of Hebei province, China. Fig. 4 shows the sketch of the 50×50 km-wide test site acquired from Google Earth. The grassland in Zhangbei is well known as "hometown of clouds" in China. It means that this area is often covered by clouds, as shown in the Google Earth image in Fig. 4. Therefore, the advantages of InSAR DEM generation technology are obvious in this area.

The test site is a part of Ba Shang grassland. The meaning of the Chinese word Ba Shang is "above a dam." In this area, the terrain rises from 1000 m to near 2000 m rapidly. The black line in the middle of the sketch in Fig. 4 flags the step-shape topography.

Figs. 5 and 6 show the unwrapped interferogram and coherence map.

The estimated phase trends are shown in Fig. 7. Because the absolute phase of interferogram is also determined in the procedure, the range of the phase trends is from 200 to 320 rad. The local APS difference, which is relative to terrain, can be seen from this figure.

Fig. 8 presents the height maps and their histograms before and after removing the phase trends. From the histogram of height map, the step-shape terrain can be clearly identified after the phase trends are removed.

Because of the satisfied baseline for DEM generation of this data set, the number of filtered pixels with gross height errors is not so large (only 40 739 of 1 416 064 pixels).

The resultant DEM is shown in Fig. 9. The left rectangle is selected for quality evaluation. In this patch, dense elevation data are collected from aerial photogrammetry as check points. A total of 2692 vector height points are shown in the
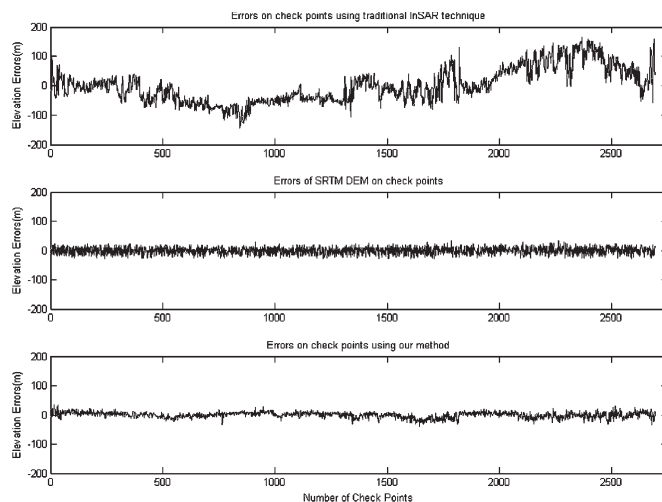
right rectangle. The elevation data are measured for generating 1/10 000 topographic map, and the accuracy is better than 2 m. The elevation values on this check points are interpolated from the resultant DEM to compare these data sets. The errors of the traditional InSAR technology, SRTM DEM, and our approach are plotted in Fig. 10. The standard deviation of the elevation errors of SRTM DEM on these check points is about 11.4 m. After phase trends removal and height map filtering, the standard deviation of elevation errors improved from 57.9 to 9.2 m and was better than the SRTM DEM.

Although the accuracy of our method is nearly the same as the SRTM DEM, the elevation data density of these two data sets should be considered. The SRTM DEM has about 90-m node distance, which is near three times of the multilooked interferogram in our experiment. In this sense, more details of surface will be reflected when the terrain is difficult to be interpolated from low-density elevation data. Therefore, the advantage of our method will be more obvious when the terrain is more complex.

B. Three Gorges Test Site

The Three Gorges region of Yangtze River in China was chosen as another test site due to its mountains with steep slopes and complex water vapor distribution. In this test site, the geometry decorrelation strongly reduces the coherence of interferogram with long baseline.

Fig. 11 shows the interferograms and their coherence maps with different baseline in this area. From this figure, the interferogram with 200-m baseline is impossible to be unwrapped successfully due to the phase aliasing, and the coherence value is much lower than the interferogram with 16-m baseline.

However, with short baselines, the phase and baseline errors would lead to large uncertainty when a DEM is constructed. The distribution of phase errors is influenced by the uncertainty of orbital parameters and APS difference of the master and slave images, as mentioned in Section I. In the case of short baselines, the height trends caused by systematic errors of interferogram will be up to useless values. These shortcomings
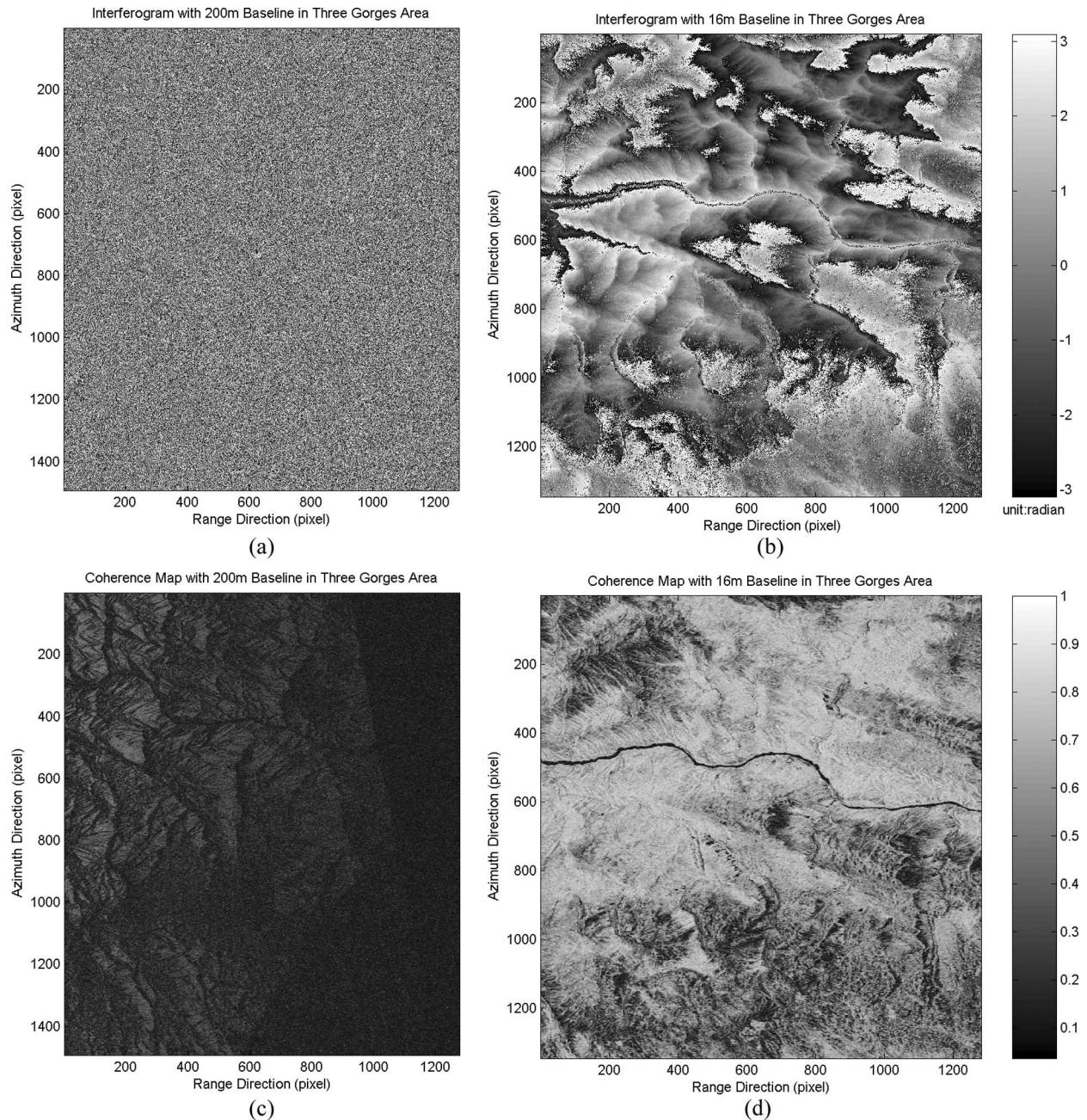
Fig. 11. Interferograms and their coherence maps with different baseline in Three Gorges area. (a) Interferogram with 200-m baseline. (b) Interferogram with 16-m baseline. (c) Coherence map of (a). (d) Coherence map of (b).

make an interferogram with high coherence, but short baseline will be scarcely used for DEM generation.

Facilitated by the SRTM DEM, the disadvantages of short baseline interferogram can be partly overcome. The following results show that the quality is improved by using the presented approach.

The procedures for data processing are the same as the ones in Zhangbei data set. The estimated phase trends in Three Gorges data set are shown in Fig. 12. Considering the baseline of this data set, if not being removed, the phase trends will cause height errors even up to thousands of meters. Therefore, the DEM from the interferogram with phase trends is not considered in the quality assessment.

The procedure for height map filtering is very important due to the short baseline. It showed that 907 711 height points among 1 725 635 pixels of the interferogram were observed with the height difference between InSAR and SRTM height values less than the estimated threshold. Although the number of points for DEM reconstruction is only about half of the whole interferogram, the terrain details are more clearly portrayed, as shown in Fig. 13.

In order to assess the quality of the DEM derived from our approach, a 1 : 50 000 DEM over the Three Gorges was used for intercomparison. This DEM was created by digitizing maps in the National Center for Geomatics of China, and the accuracy of grid nodes is claimed to be 11 m in mountainous region.
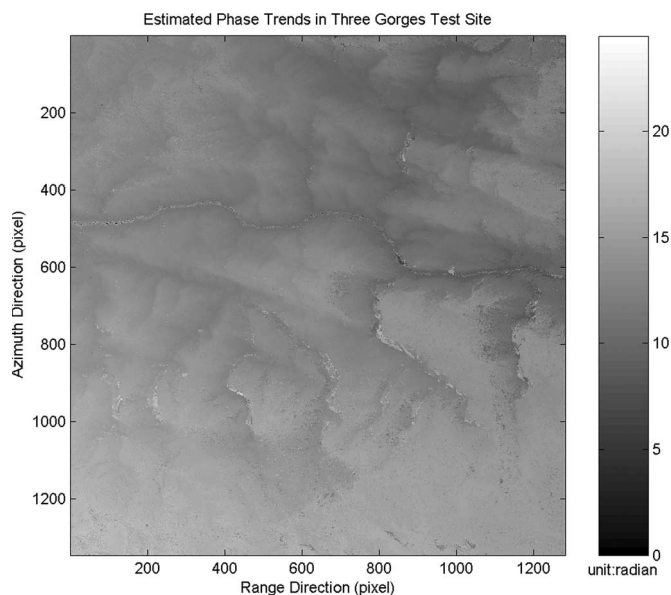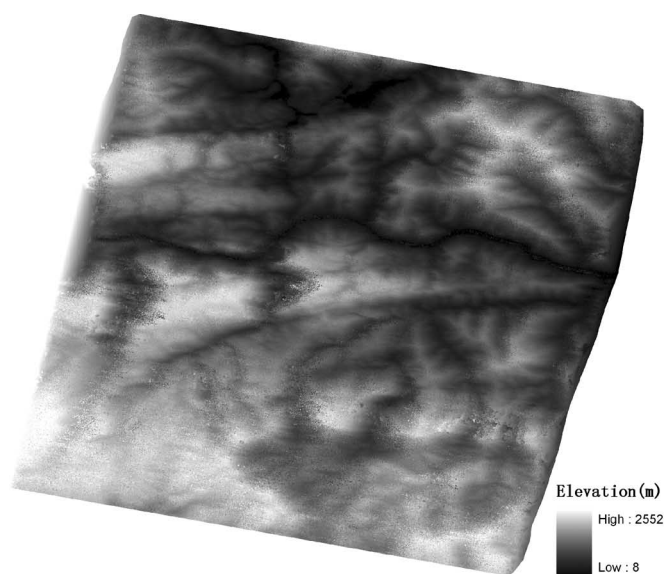
Fig. 12.   Estimated phase trends of Three Gorges data set.

(a)

(b)

Fig. 13.   Comparison of DEMs before and after filtering gross errors of Three Gorges data set. The white rectangle indicates the profile analysis area. (a) DEM before filtering gross errors. (b) DEM after filtering gross errors.

Due to the lack of high-accuracy DEMs or check points in this test site, the comparison among the DEMs is performed on two profile lines. Fig. 14 plots the profile analysis among 1 : 50 000 DEM, and the InSAR DEM before filtering gross errors and after filtering gross errors of the Three Gorges area. From this figure, the high frequency errors caused by gross height errors are strongly reduced.

Because of the steep terrain, some radar shadow areas strongly affect the error standard deviation (about 50 m), which is calculated from the elevation difference between the resulted DEM and 1 : 50 000 DEM. Also, the horizontal errors while converting the InSAR-derived DEM into map project (Xi'an geodetic coordinate system 1980 of China) carry certain elevation errors caused by the horizontal errors as well. However, as shown in Figs. 13 and 14, the quality improvement using our approach is obvious.

V. CONCLUSION

In this paper, an approach for DEM construction from ERS Tandem data is presented. The SRTM DEM is used as external DEM data to model and remove symmetrical phase errors and APS difference. Another advantage of the presented approach is that, before interpolating the resulting DEM from the InSAR height map, pixels with gross height errors can be removed by the threshold derived from the SRTM DEM. Experimental results in two test sites proved the potential of our approach in reducing phase errors and APS difference. Taking into account the steep slopes, the improvement of standard deviation of elevation errors is remarkable. Since the SRTM has opened the world wide 3 arc-seconds resolution DEMs and made them downloadable from Internet, this new approach provides an effective tool to make use of existing low-resolution DEMs in interested cloud-covered and rainy areas, which are hardly observed by optic technology. Also, one can obtain high resolution and quality DEMs from InSAR data sets and other external
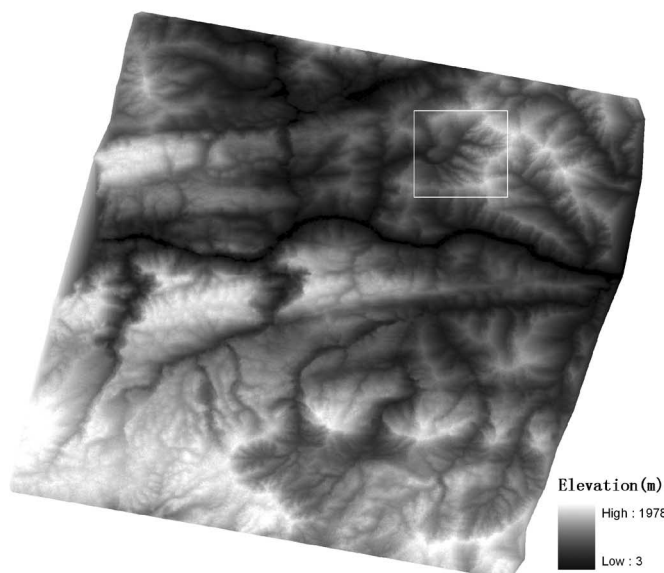
DEM such as 1 : 100 000 scale DEMs or even DEMs with lower resolution by our approach. Finally, taken as our future work, the research about the usage of phase trends model in short-term two-pass D-InSAR processing has been developing.
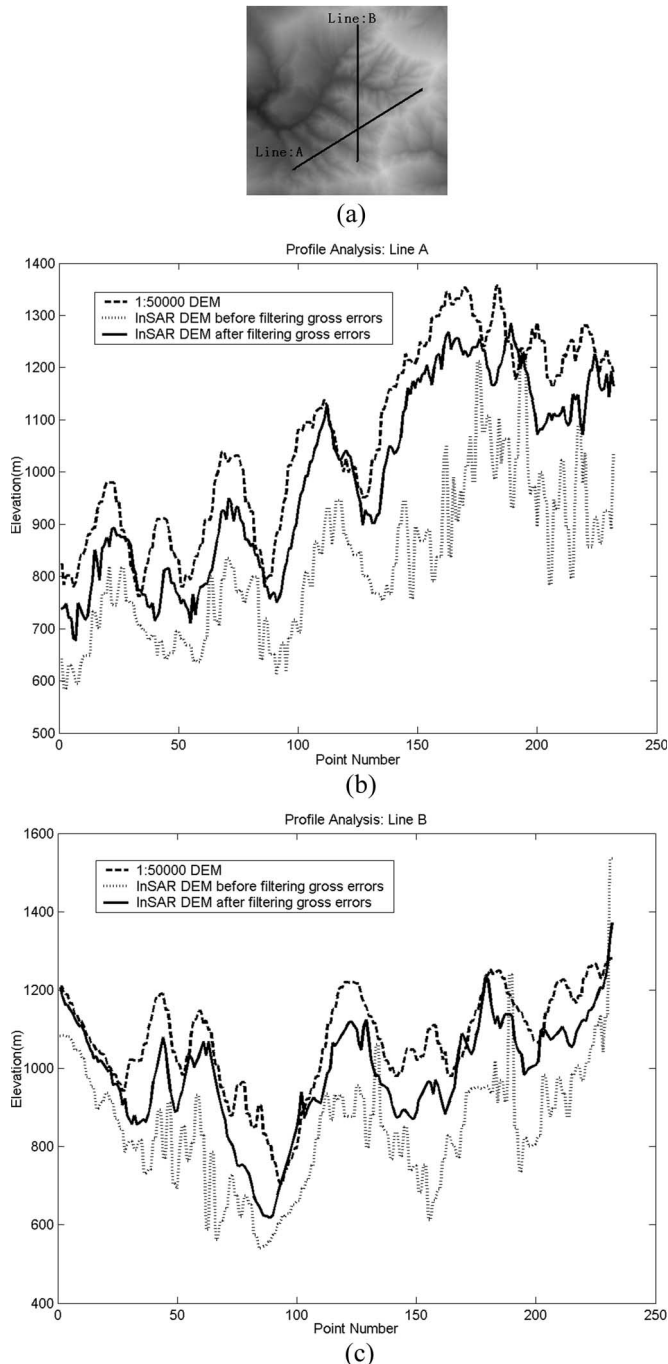
(a)

(b)

(c)

Fig. 14.　Profile analysis among 1 : 50 000 DEM, and the InSAR DEM before filtering gross errors and after filtering gross errors of Three Gorges area. (a) Sketch map of two profile lines. (b) Profile line A. (c) Profile line B.

REFERENCES

[1] H. A. Zebker and R. M. Goldstein, "Topographic mapping from interferometric synthetic aperture radar observations," *J. Geophys. Res.*, vol. 91, no. B5, pp. 4993–4999, 1986.

[2] H. A. Zebker, C. L. Werner, P. A. Rosen, and S. Hensley, "Accuracy of topographic maps derived from ERS-1 interferometric radar," *IEEE Trans. Geosci. Remote Sens.*, vol. 32, no. 4, pp. 823–836, Jul. 1994.

[3] P. A. Rosen, S. Hensley, I. R. Joughin, F. K. Li, S. N. Madsen, E. Rodriguez, and R. M. Goldstein, "Synthetic aperture radar interferometry," *Proc. IEEE*, vol. 88, no. 3, pp. 333–382, Mar. 2000.

[4] H. A. Zebker and J. Villasenor, "Decorrelation in interferometric radar echoes," *IEEE Trans. Geosci. Remote Sens.*, vol. 30, no. 5, pp. 950–959, Sep. 1992.

[5] R. F. Hanssen, *Radar Interferometry Data Interpretation and Error Analysis.*　Dordrecht, The Netherlands: Kluwer, 2001.

[6] R. Goldstein, "Atmospheric limitations to repeat-pass interferometry," *Geophys. Res. Lett.*, vol. 22, no. 18, pp. 2517–2520, Sep. 1995.

[7] A. Ferretti, C. Prati, and F. Rocca, "Multibaseline InSAR DEM reconstruction: The wavelet approach," *IEEE Trans. Geosci. Remote Sens.*, vol. 37, no. 2, pp. 705–715, Mar. 1999.

[8] S. N. Madsen, H. A. Zebker, and J. Martin, "Topographic mapping using radar interferometry: Processing techniques," *IEEE Trans. Geosci. Remote Sens.*, vol. 31, no. 1, pp. 246–256, Jan. 1993.

[9] M. S. Seymour and I. G. Cumming, "InSAR terrain height estimation using low-quality sparse DEM's," in *Proc. 3rd ERS Symp.*, Florence, Italy, 1997, pp. 421–426. [Online]. Available: http://florence97.ers-symposium.org/

[10] M. Eineder and N. Adam, "A maximum-likelihood estimator to simultaneously unwrap, geocode, and fuse SAR interferograms from different viewing geometries into one digital elevation model," *IEEE Trans. Geosci. Remote Sens.*, vol. 43, no. 1, pp. 24–36, Jan. 2005.

[11] S.-H. Yun, J. Ji, H. Zebker, and P. Segall, "On merging high- and low-resolution DEMs from TOPSAR and SRTM using a prediction-error filter," *IEEE Trans. Geosci. Remote Sens.*, vol. 43, no. 7, pp. 1682–1690, Jul. 2005.

[12] Jet Propulsion Laboratory. (2005, Aug. 28). *Shuttle Radar Topography Mission: Mission Overview.* [Online]. Available: http://www2.jpl.nasa.gov/srtm/missionoverview.html

[13] G. Schreier, *SAR Geocoding: Data and Systems.*　Heidelberg, Germany: Herbert Wichmann Verlag, 1993.

[14] B. Kampes and S. Usai, "Doris: The Delft object-oriented radar interferometric software," in *Proc. ITC 2nd ORS Symp.*, Aug. 1999, pp. 241–244. [CD-ROM].

[15] M. S. Seymour and I. G. Cumming, "Maximum likelihood estimation for SAR interferometry," in *Proc. IGARSS*, Pasadena, CA, 1994, pp. 2272–2275.

[16] Z. Li, Q. Zhu, and G. Chris, *Digital Terrain Modeling: Principles and Methodology.*　Boca Raton, FL: CRC Press, 2004.

[17] D. C. Ghighlia and M. D. Pritt, *Two-Dimensional Phase Unwrapping: Theory, Algorithms, and Software.*　New York: Wiley, 1998.

[18] T. J. Flynn, "Two-dimension phase unwrapping with minimum weighted discontinuity," *J. Opt. Soc. Amer. A, Opt. Image Sci.*, vol. 14, no. 10, pp. 2692–2701, Oct. 1997.

[19] B. Smith and D. Sandwell, "Accuracy and resolution of shuttle radar topography mission data," *Geophys. Res. Lett.*, vol. 30, no. 9, pp. 1467–1470, 2003.
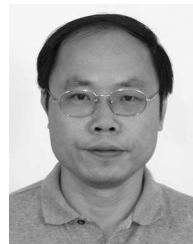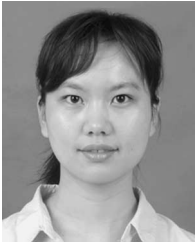
Mingsheng Liao received the M.Eng. degree in electronic engineering and the Ph.D. degree in photogrammetry and remote sensing from Wuhan Technical University of Surveying and Mapping (WTUSM), Wuhan, China, in 1985 and 2000, respectively.

From 1985 to 1992, he was with the Department of Electronic Engineering, WTUSM, which is one of the universities that formed Wuhan University in 2000. From 1992 to 2000, he was with the State Key Laboratory for Information Engineering in Surveying, Mapping and Remote Sensing (LIESMARS), WTUSM, and obtained a Professorship in 1997. Between 1995 and 1996, he was with the Department of Surveying and Photogrammetry, Technical University of Denmark, as a visiting Ph.D. candidate. From 2000 to 2002, he was with the Joint Laboratory for Geo-information Science, Chinese University of Hong Kong, as a Research Associate. Since 2003, he has been at the LIESMARS, Wuhan University, where he is leading the SAR data analysis and processing group. His main research interests are in interferometric and polarimetric data processing, differential SAR interferometry, and multitemporal SAR image analysis. He has more than 50 publications in international journals, conferences, and workshops.
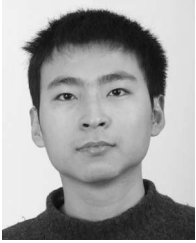
Teng Wang received the M.Eng. degree in photogrammetry and remote sensing from Wuhan University, Wuhan, China, in 2006. He is currently working toward the Ph.D. degree in SAR interferometry fields at the State Key Laboratory for Information Engineering in Surveying, Mapping and Remote Sensing, Wuhan University, Wuhan, and Dipartimento di Elettronica e Informazione, Politecnico di Milano, Milan, Italy.

His current research interests include the digital elevation model generation by InSAR and PS InSAR technology in mountainous areas.

Lijun Lu received the M.Eng. degree in photogrammetry and remote sensing from Wuhan University, Wuhan, China, in 2006. She is currently working toward the Ph.D. degree in SAR interferometry fields at the State Key Laboratory for Information Engineering in Surveying, Mapping and Remote Sensing, Wuhan University, Wuhan.

Her current research interests include the permanent scatterer interferometry and target detection.

Wenjun Zhou received the B.Eng. degree from Wuhan Technical University of Surveying and Mapping, Wuhan, China, and the M.Eng. degree from Wuhan University, Wuhan, in 1997 and 2006, respectively.

Since 1997, he has been working in the Third Institute of Surveying and Mapping of Hebei Province, Shijiazhuang, China. His current work is in the field of digital elevation model and digital orthomap production.

Deren Li received the Master degree in photogrammetry and remote sensing from Wuhan Technical University of Surveying and Mapping (WTUSM), Wuhan, China, in 1981, and the Ph.D. degree from Stuttgart University, Stuttgart, Germany, in 1985.

From 1997 to 2000, he was the President of WTUSM. From 2000 to 2006, he was the Director of the State Key Laboratory for Information Engineering in Surveying, Mapping and Remote Sensing, Wuhan University, Wuhan. Since 1990, he has been concentrating on the research and education in geospatial information science and technology represented by remote sensing, global positioning system, and geographic information system.

Prof. Li is a member of the Chinese Academy of Sciences and the Chinese Academy of Engineering. He is also a member of the Euro-Asia International Academy of Science.